The Astrophysical Journal, 804:30 (14pp), 2015 May 1 doi:10.1088/0004-637X/804/1/30

MULTIPLICITY OF THE GALACTIC SENIOR CITIZENS: A HIGH-RESOLUTION SEARCH FOR COOL SUBDWARF COMPANIONS

Carl Ziegler[1], Nicholas M. Law[1], Christoph Baranec[2], Reed L. Riddle[3], and Joshua T. Fuchs[1]
[1] Department of Physics and Astronomy, University of North Carolina at Chapel Hill, Chapel Hill, NC 27599-3255, USA; carlziegler@unc.edu
[2] Institute for Astronomy, University of Hawai'i at Mānoa, HI 96720-2700, USA
[3] Division of Physics, Mathematics, and Astronomy, California Institute of Technology, Pasadena, CA 91125, USA
Received 2014 November 11; accepted 2015 February 16; published 2015 April 27

ABSTRACT

Cool subdwarfs are the oldest members of the low-mass stellar population. Mostly present in the galactic halo, subdwarfs are characterized by their low-metallicity. Measuring their binary fraction and comparing it to solar-metallicity stars could give key insights into the star formation process early in the Milky Way's history. However, because of their low luminosity and relative rarity in the solar neighborhood, binarity surveys of cool subdwarfs have suffered from small sample sizes and incompleteness. Previous surveys have suggested that the binary fraction of red subdwarfs is much lower than for their main-sequence cousins. Using the highly efficient Robo-AO system, we present the largest high-resolution survey of subdwarfs, sensitive to angular separations ($\rho \geqslant 0\farcs15$) and contrast ratios ($\Delta m_i \leqslant 6$) invisible in past surveys. Of 344 target cool subdwarfs, 43 are in multiple systems, 19 of which are newly discovered, for a binary fraction of $12.5 \pm 1.9\%$. We also discovered seven triple star systems for a triplet fraction of $2.0 \pm 0.8\%$. Comparisons to similar surveys of solar-metallicity dwarf stars gives a $\sim 3\sigma$ disparity in luminosity between companion stars, with subdwarfs displaying a shortage of low-contrast companions. We also observe a lack of close subdwarf companions in comparison to similar-mass dwarf multiple systems.

Key words: binaries: close – instrumentation: adaptive optics – methods: data analysis – stars: late-type – subdwarfs – techniques: high angular resolution

1. INTRODUCTION

Cool subdwarfs are the oldest members of the low-mass stellar population, with spectral types of G, K, and M, masses between ~0.6 and ~0.08 $M_\odot$, and surface effective temperatures between 4000 and 2300 K (Kaltenegger & Traub 2009). First coined by Kuiper (1939), subdwarfs are the low-luminosity, metal-poor ([Fe/H] < -1) spectral counterparts to the main sequence dwarfs. On a color–magnitude diagram, subdwarfs lie between white dwarfs and the main sequence (Adams 1915). With decreased metal opacity, subdwarfs have smaller stellar radii and are bluer at a given luminosity than their main sequence counterparts (Sandage & Eggen 1959). These low-mass stars are members of the Galactic halo (Gould 2003) and have higher systematic velocities and proper motions than disk dwarf stars. Traditionally subdwarfs have been identified using high proper motion surveys. Although 99.7% of stars in the galaxy are disk main sequence, statistically there are more subdwarfs in these high PM surveys (Reid & Hawley 2005). Verification and precise spectral typing of cool subdwarfs can be performed by measuring molecular lines, as defined first by Gizis (1997). Lépine et al. (2007) introduced a refined system, using spectroscopic measurements of a large 1983 star survey to standardize the subdwarf metallicity subclasses and spectroscopic sequence.

The search for companions to stars of different masses gives clues to the star formation process, as any successful model must account for both the frequency of the multiple star systems and the properties of the systems. In addition, monitoring the orbital characteristics of multiple star systems yields information otherwise unattainable for single stars, such as relative brightness and masses of the components (Goodwin et al. 2007), lending further constraints to mass–luminosity relationships (Chabrier et al. 2000).

Old population II stars are important probes for the early history of star formation in the galaxy (Zhang et al. 2013). The formation process of low-mass stars remains less well understood than for solar-like stars. Although multiple indications suggest they form as the low-mass tail of regular star formation (Bourke et al. 2006), other mechanisms have been proposed for some or all of these objects (Goodwin & Whitworth 2007; Thies & Kroupa 2007; Basu & Vorobyov 2012). A firm binary fraction for low-metallicity cool stars could assist in constraining various formation models. This again motivates the need for a comprehensive binarity survey, sensitive to small angular separations.

The multiplicity of main sequence dwarfs has been well explored in the literature. A consistent trend that has purveyed is that the percentage of stars with stellar companions seems to depend on the mass of the stars. For AB-type stars, Peter et al. (2012) used a sample of 148 stars to determine a companion fraction of ~70%. For solar type stars (FGK-type), around 57% have companions (Duquennoy & Mayor 1991), although Raghavan et al. (2010) have revised the fraction down to ~46%. Fischer & Marcy (1992) looked at M-dwarfs and found a multiplicity fraction of $42 \pm 9\%$. More recently, Janson et al. (2012) found a binary fraction for late K- to mid M-type dwarfs of $27 \pm 3\%$ from a sample of 701 stars. For late M-dwarfs, a slightly lower fraction was found by Law et al. (2006b) of $7\% \pm 3\%$. Extending their previous study for mid/late M-type dwarfs, M5–M8, Janson et al. (2014) find a multiplicity fraction of 21%–27% using a sample of 205 stars.

While the multiplicity of dwarf stars has been heavily studied with comprehensive surveys, detailed multiplicity studies of low-mass subdwarfs have, historically, been hindered by their low luminosities and relative rarity in the solar neighborhood. Within 10 pc, there are three low-mass subdwarfs, compared to

243 main sequence stars (Monteiro et al. 2006). Subsequently, multiplicity surveys of cool subdwarfs have been relatively small. The largest, a low-limit angular resolution search by Zhang et al. (2013) mined the Sloan Digital Sky Survey (SDSS; York et al. 2000) to find 1826 cool subdwarfs, picking out subdwarfs by their PMs and identifying spectral type by fitting an absolute magnitude-spectral type relationship. They find 45 subdwarfs multiple systems in total, with 30 being wide companions and 15 partially resolved companions. When adjusting for the incompleteness of their survey, an estimate of the binary fraction of >10% is predicted. The authors note the need for a high spatial resolution imaging survey to search for close binaries (<100 AU) and put tighter constraints on the binary fraction of cool subdwarfs.

The high-resolution subdwarf surveys completed thus far have been comparatively small. Gizis & Reid (2000) detected no companions in a sample of eleven cool subdwarfs. Riaz et al. (2008) similarly found no companions in a sample of 19 M-subdwarfs using the *Hubble Space Telescope*. Lodieu et al. (2009) reported one companion in a sample of 33 M type subdwarfs. Jao et al. (2009) found four companions in a sample of 62 cool subdwarf systems. With the high variance in small number statistics, the relationship between dwarf and subdwarf multiplicity fractions remains inconclusive.

We present here the largest high resolution cool subdwarf multiplicity survey yet performed, making use of the efficient Robo-AO system (Baranec et al. 2014). The Robo-AO system allows us to detect more cool and close companion stars in a much larger sample size than previously possible. This survey combines previously known wide proper-motion pairs, spectroscopic binaries, and high angular resolution images able to detect companions with $\rho \geqslant 0\farcs15$ and $\Delta m_i \leqslant 6$.

The paper is organized as follows. In Section 2 we describe the target selection, the Robo-AO system, and follow-up observations. In Section 3 we describe the Robo-AO data reduction and the companion detection and analysis. In Section 4 we describe the results of this survey, including discovered companions, and compare to similar dwarf surveys. The results are discussed in Section 5 and put in context of previous literature. We conclude in Section 6.

2. SURVEY TARGETS AND OBSERVATIONS

2.1. Sample Selection

We selected targets from the 564 spectral type F- through M-subdwarf candidates studied by Marshall (2007). These targets were selected from the New Luyten Two-Tenths catalog (NLTT; Luyten 1979; Luyten & Hughes 1980) of high proper motion stars (>0.18 arcsec yr^{-1}) using a reduced proper motion diagram (RPM). To distinguish subdwarf stars from their solar-metallicity companions on the main sequence, the RPM used a $(V - J)$ optical–infrared baseline, a technique first used by Salim & Gould (2002), rather than the shorter $(B - R)$ baseline used by Luyten. This method uses the high proper motion as a proxy for distance and the blueness of subdwarfs relative to equal luminosity dwarf stars to separate out main sequence members of the local disk and the halo subdwarfs (Marshall 2008). The RPM, H_M, is defined as

$$H_M = m + 5 \log \mu + 5 \quad (1)$$

where m is the apparent magnitude and μ is the proper motion in $''$/yr. The discriminator, η, developed by Salim and Gould to separate luminosity classes, is defined as

$$\eta(H_V, V - J, \sin b) = H_V - 3.1(V - J) - 1.47\,|\sin b| - 7.73 \quad (2)$$

where b is the Galactic latitude. The RPM diagram for the revised NLTT (rNLTT) catalog (Gould & Salim 2003) and our subdwarf targets is presented in Figure 1. The improved photometry of Marshall (2007) placed 12 of the original suspected subdwarfs outside the subdwarf sequence. These stars were not included in our sample. Possible dwarf contamination of our sample is expected to be small, as described in Section 3.3. Of the 552 subdwarfs confirmed by Marshall, a randomly selected sample of 348 G-, K-, and M-subdwarfs were observed by Robo-AO when available between other high priority surveys. The V-band magnitudes and $(V - J)$ colors of the observed subdwarf sample are shown in Figure 2.

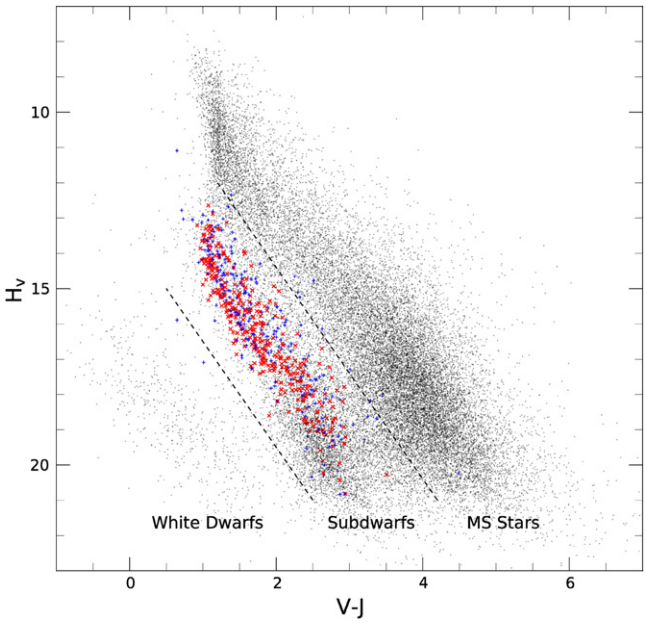

Figure 1. Reduced proper motion diagram of the complete rNLTT (Gould & Salim 2003), with our observed subdwarfs in red *X*'s, drawn from the photometric work of Marshall (2007). Unobserved candidate subdwarfs from Marshall (2007) are plotted as blue +'s. The discriminator lines, described in Section 2.1, between solar-metallicity dwarfs, metal-poor subdwarfs, and white dwarfs are at $\eta = 0$ and 5.15, respectively, and with $b = \pm 30$. The subdwarfs plotted make use of the improved photometry of Marshall (2007).

2.2. Observations

2.2.1. Robo-AO

We obtained high-angular-resolution images of the 348 subdwarfs during 32 separate nights of observations between 2012 September 3 and 2013 August 21 (UT). The observations were performed using the Robo-AO laser adaptive optics system (Riddle et al. 2012; Baranec et al. 2013, 2014) mounted on the Palomar 60 inch telescope. The first robotic laser guide star adaptive optics system, the automatic Robo-AO system can efficiently observe large, high-resolution surveys. All images were taken using the Sloan i'-band filter (York et al. 2000) and with exposure times of 120 s. Typical seeing at the Palomar Observatory is between $0\farcs8$ and $1\farcs8$, with the median around $1\farcs1$ (Baranec et al. 2014). The typical FWHM (diffraction

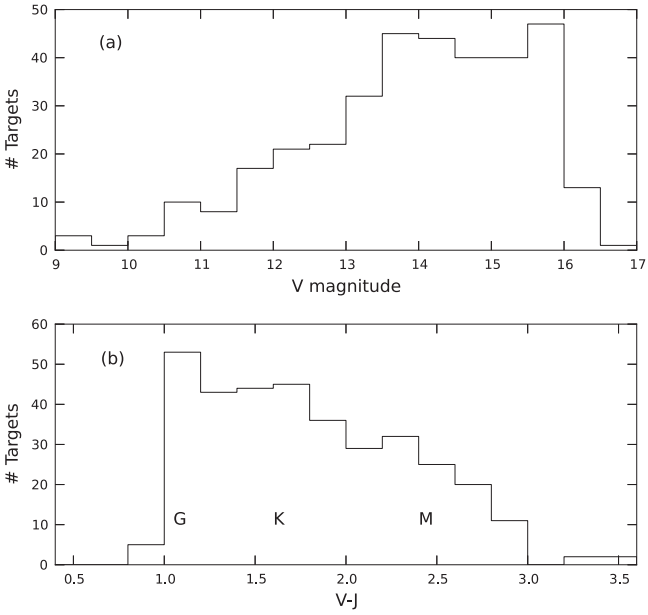

Figure 2. (a) Histogram of magnitudes in V-band of the 348 observed subdwarfs. (b) Histogram of the $(V - J)$ colors of the observed subdwarf sample, with approximate spectral types regions G, K, and M marked, using the spectral color indices of Ducati et al. (2001). Both plots use the photometry of Marshall (2007).

Table 1
The Specifications of the Robo-AO Subdwarf Survey

Filter	Sloan i'-band
FWHM resolution	0.″15
Field size	44″ × 44″
Detector format	1024^2 pixels
Pixel scale	43.1 mas/pix
Exposure time	120 s
Subdwarf targets	344
Targets observed/hour	20
Observation dates	2012 Sep 1–2013 Aug 21

limited) resolution of the Robo-AO system is 0.″12–0.″15. Images are recorded on an electron-multiplying CCD (EMCCD), allowing short frame rates for tip and tilt correction in software using a natural guide star ($m_V < 16$) in the field of view (FOV). Specifications of the Robo-AO system are summarized in Table 1.

The images were reduced by the Robo-AO imaging pipeline described in Law et al. (2009, 2014). The EMCCD output frames are dark-subtracted and flat-fielded and then, using the Drizzle algorithm (Fruchter & Hook 2002), stacked and aligned, while correcting for image motion using a star in the field. The algorithm also introduces a factor of 2 up-sampling to the images. Since the subdwarf targets are in relatively sparse stellar fields, for the majority of the images the only star visible is the target star and it was thus used to correct for the image motion.

2.2.2. Keck LGS-AO

Six candidate multiple systems were selected for re-imaging by the NIRC2 camera behind the Keck II laser guide star adaptive optics system (van Dam et al. 2006; Wizinowich et al. 2006), on 2014 August 17 (UT) to confirm possible companions. The targets were selected for their low significance of detectability, either because of low contrast ratio or small angular separation. The observations were done in the K'- and H-bands with three 90 s exposures for two targets and three 30 s exposures for five targets in a three-position dither pattern that avoided the noisy, lower-left quadrant. We used the narrow camera setting (0.″0099/px), which gave a single-frame FOV of 10″ × 10″.

2.2.3. SOAR Goodman Spectroscopy

We took spectra of 24 of the subdwarfs using the Southern Astrophysical Research Telescope (SOAR) and the Goodman Spectrograph (Clemens et al. 2004) on 2014 July 15. We observed 12 targets with companions and 12 single stars from the subdwarf sample as reference. The spectra were taken using a 930 lines/mm grating with 0.42 Å/pixel, a 1.″07 slit, and exposure times of 480 s.

3. DATA REDUCTION AND ANALYSIS

3.1. Robo-AO Imaging

3.1.1. Target Verification

To verify that each star viewed in the image is the desired subdwarf target, we created Digital Sky Survey cutouts of similar angular size around the target coordinates. Each image was then manually checked to assure no ambiguity in the target star. The vast majority of the targets are in relatively sparse stellar regions. Four of the target stars in crowded fields whose identification was ambiguous were discarded, leaving 344 verified subdwarf targets.

3.1.2. Point-spread Function (PSF) Subtraction

To locate close companions, a custom locally optimized PSF subtraction routine (Law et al. 2014) based on the Locally Optimized Combination of Images algorithm (Lafrenière et al. 2007) was applied to centered cutouts of all stars. Successful PSF subtraction requires similar reference images, taken at similar times, with similar instruments, and with reference stars of similar brightnesses. The set of subdwarf observations taken at similar times meet these criteria and were used as references, instead of dedicated reference observations, thus optimizing survey efficiency. This is made possible by the improbability of having a companion in the same position for two different targets.

For each target image and for 20 reference images selected as the closest to the target image in observation time, the region around the star was subdivided into polar sections, five up-sampled pixels in radius and 45° in angle. A locally optimized estimate of the PSF for each section was then generated using a linear combination of the reference PSFs. The algorithm begins with an average over the reference PSFs, then uses a downhill simplex algorithm to optimize the contributions from each reference image to find the best fit to the target image. The optimization is done on several coincident sections simultaneously to minimize the probability of subtracting out a real companion, with only the central region outputted to the final PSF. This also provides smoother transitions between adjacent sections as many of the image pixels were shared in the optimization.

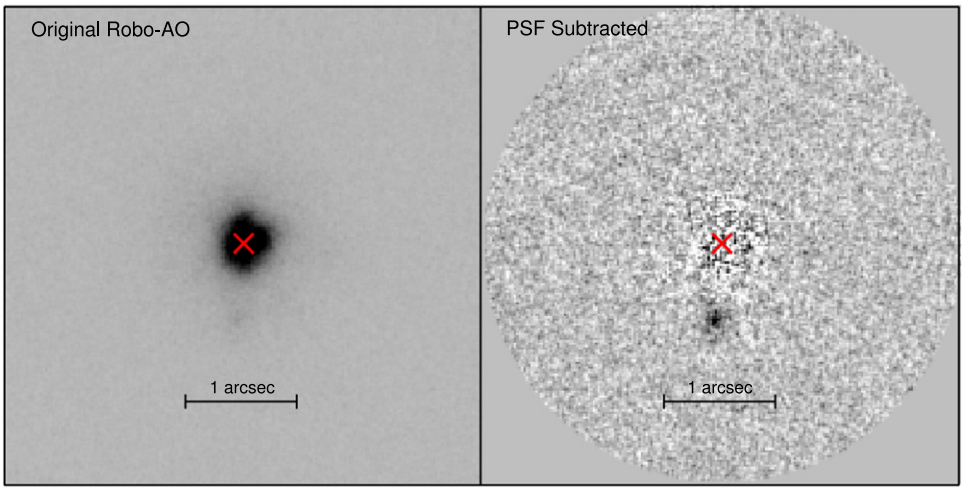

Figure 3. Example of PSF subtraction on NLTT 31240 with companion separation of 0.″74. The red × marks the position of the primary star's PSF peak. Successful removal of the PSF leaves residuals consistent with photon noise.

After iterating over all sections of the image, the final PSF is an optimal local combination of all the reference PSFs. This final PSF is then subtracted from the original reference image, leaving residuals that are consistent with photon noise. Figure 3 shows an example of the PSF subtraction performance.

We ran the PSF subtraction algorithm on all our targets out to a radius of 2″. We subsequently reran the automated companion detection routine on the subtracted images to find significant ($>5\sigma$) close companions, and manually checked the results.

3.1.3. Automated Companion Detection

To efficiently find companions in the large data set, we developed a custom search algorithm, based on the method described in Law et al. (2014). The algorithm searches every four-pixel diameter aperture in the image and compares the signal inside the aperture to the average noise level at that radius from the target star. The detected companions were then manually checked, eliminating spurious detections with dissimilar PSFs to the target star and those having characteristics of a cosmic ray hit, such as a single bright pixel or bright streak. The detection significance of found companions is listed in Table 4.

3.1.4. Imaging Performance Metrics

The two dominant factors that effect the image performance of the Robo-AO system are seeing and target brightness. To further classify the image performance for each target an automated routine was ran on all images. Described in detail in Law et al. (2014), the code uses two Moffat functions fit to the PSF to separate the widths of the core and halo. We found that the core size was an excellent predictor of the contrast performance, and used it to group targets into three levels (low, medium, and high). Counter-intuitively, the PSF core size decreases as image quality decreases. This is caused by poor signal-to-noise ratio on the shift-and-add image alignment used by the EMCCD detector. The frame alignment subsequently locks onto photon noise spikes, leading to single-pixel-sized spikes in the images (Law et al. 2006b, 2009). The images with diffraction limited core size (∼0.″15) were assigned to the high-performance group, with smaller cores assigned to lower-performance groups. For our target observations, 32% fall in the low performance group, 43% in the medium performance group, and 25% in the high performance group.

Using a companion-detection simulation with a group of representative targets, we determine the angular separation and contrast consistent with a 5σ detection. For clarity, the contrast curves of the simulated targets are fitted with functions of the form $a - b/(r - c)$ (where r is the radius from the target star and a, b, and c are fitting variables). Contrast curves for the three performance groups are shown in Section 5 in Figure 9 passing reference.

3.1.5. Contrast Ratios

For wide companions, the binaries' contrast ratio was determined using aperture photometry on the original images. The aperture size was determined uniquely for each system based on separation and the presence of non-associated background stars.

For close companions, the estimated PSF was used to remove the blended contributions of each star before aperture photometry was performed. The locally optimized PSF subtraction algorithm attempts to remove the flux from companions using other reference PSFs with excess brightness in those areas. For detection purposes, we use many PSF core sizes for optimization, and the algorithm's ability to remove the companion light is reduced. However, the companion is artificially faint as some flux has still been subtracted. To avoid this, the PSF fit was redone excluding a six-pixel-diameter region around the detected companion. The large PSF regions allow the excess light from the primary star to be removed, while not reducing the brightness of the companion.

3.1.6. Separation and Position Angles

Separation angles were determined from the raw pixel positions. Uncertainties were found using estimated systematic errors due to blending between components. Typical uncertainty in the position for each star was 1–2 pixels. Position angles were calculated using a distortion solution produced using Robo-AO measurements for a globular cluster.[4]

[4] S. Hildebrandt (2013, private communication).

3.2. Previously Detected Binaries

To further realize our goal of a comprehensive cool subdwarf survey, we included in our statistics previously confirmed binary systems in the literature with separations outside of our FOV. Common proper motion is a useful indicator of wider binary systems. Wide (>30″) common proper motion companions among our target subdwarfs were previously identified in the Revised New Luyten Two-Tenths catalog (rNLTT; Salim & Gould 2002; Chanamé & Gould 2004), and a search by López et al. (2012) of the Lepine and Shara Proper Motion-North catalog (LSPM) (Lépine & Shara 2005). None of our target stars overlap with the large survey of (Zhang et al. 2013), as our targets are several magnitudes brighter on average.

The target list was also cross-checked against the *Ninth Catalogue of Spectroscopic Binary Orbits* (S_{B^9}; Pourbaix et al. 2004), a catalog of known spectroscopic binaries available online.[5] While these systems were included in the total subdwarf binary numbers, the compilatory nature of this catalog leaves some uncertainty in the completeness of the spectroscopic search.

3.3. Spectroscopy

To further verify that the targets selected are cool subdwarfs, we took spectra of 7% of the total survey and 31% of the candidate companion systems. Past spectroscopic studies of cool subdwarfs at high resolution have proven difficult as, at the low temperatures present, a forest of molecular absorption lines conceals most atomic lines used in spectral analysis. Subdwarfs can be classified spectroscopically using two molecular lines (Gizis 1997). Comparing titanium oxide (TiO) bands to metal hydride bands (typically CaH in M-subdwarfs), Gizis classified two groups, the intermediate and extreme subdwarfs. As the metallicity decreases, the TiO adsorption also decreases, but the CaH remains largely unaffected for a given spectral type. This classification system was expanded and revised to include ultra subdwarfs by Lépine et al. (2007), who introduced the new useful parameter $\zeta_{TiO/CaH}$.

Spectra were taken for wavelengths 5900–7400 Å, and reduced (dark-subtracted and flat-fielded) using IRAF reduction packages, particularly onedspec.apall to extract the trace of the spectrum and onedspec.dispcor for applying the wavelength calibration. A Fe+Ar arc lamp was recorded for wavelength calibration. All observed target subdwarfs were confirmed to show the spectral characteristics of subdwarf stars described above, specifically the reduced band strength of 7050 Å TiO5. An example of the extracted spectra is given in Figure 4. The full observation list for SOAR is given in Table 2.

With all 24 sampled subdwarfs confirmed, spectroscopy alone gives a 95% confidence limit that the fractional dwarf contamination is below 0.12; the most likely contamination (50th percentile) below 0.03. This does not account, however, for the targets placement on a RPM diagram, which also suggests that the stars are in fact subdwarfs. We expect that the dwarf contamination is thus also lower than the small spectroscopic sample implies. We therefore consider targets not yet observed by SOAR to be probable, although unconfirmed, subdwarfs.

[5] http://sb9.astro.ulb.ac.be/

3.4. Candidate Companion Follow-ups

With either high contrast ratio or small angular separation, seven candidate subdwarf binary systems with low detection significance (<6σ) were selected for follow-up imaging using Keck II. One low-probability candidate companion star was rejected after followups using Keck II, an apparent close ($\rho \simeq 0\farcs15$) binary to NLTT 50869, probably resulting from a cosmic ray on the original Robo-AO image. A wider binary to NLTT 50869, with high detection significance, was not in the image FOV. Outside of the six target stars with low significantce companions, another candidate companion star, NLTT 4817, was observed and had no companion inside the FOV of the Keck II image; however, it had a high significance companion (>7σ) in the Robo-AO FOV. An example of the Keck II images and the Robo-AO images is given in Figure 5. The full Keck II observations are listed in Table 3, with the second to last column indicating the presence of companion and the last column the *H*-band magnitude difference of the companion. Angular separations for the companions are listed in Table 4. Confirmed companions and contrast curve for the Keck images are plotted in Figure 6. The area under the contrast curve was searched for all Keck images and was free of additional companions.

4. DISCOVERIES

Of the 344 verified subdwarf targets observed, 43 appear to be in multiple star systems for an apparent binary fraction of 12.5 ± 1.9%, where the error is based on Poissonian statistics (Burgasser et al. 2003). This count includes six multiple systems first recorded in the NLTT, 13 systems first recorded in the rNLTT, one wide binary found in the LSPM (López et al. 2012), six spectroscopic binaries, and 19 newly discovered multiple systems. We also found five new companions to already recorded binary systems, including two new triple systems, for a total of seven triple star systems, for a triplet fraction of 2.0 ± 0.8%. One quarter (26%) of the companions would only be observable in a high-resolution survey (<2.″0 separation). The overarching dwarf trend of decreased binary fraction with later spectral types is not apparent for our sample of subdwarfs. This is seen in Figure 7, where the binary fraction of the target stars binned by their $(V - J)$ color is presented. Cutouts of the closest 22 multiple star systems are shown in Figure 8. Measured companion properties are detailed in Table 4.

4.1. Probability of Association

The associations of all discovered and previously recorded companions were confirmed using the DSS (Reid et al. 1991), of the POSS-I (Abell 1959). Since all the targets have high proper motions, if not physically associated the systems would have highly apparent shifts in separation and position angle over the past six decades. For the widely separated systems with both stars visible in the DSS, we checked the angular separation in the DSS and our survey to confirm relatively constant separation. For closely separated systems where both stars are merged in the DSS, we looked for a background star at the current position that does not appear in our images.

With the majority of POSS-I archival images taken between between 1949 and 1956 and scanned with plate scale of 1″/px, we can dissociate stars in the field with proper motion differences of >16 mas yr^{-1}, and proper motion differences in

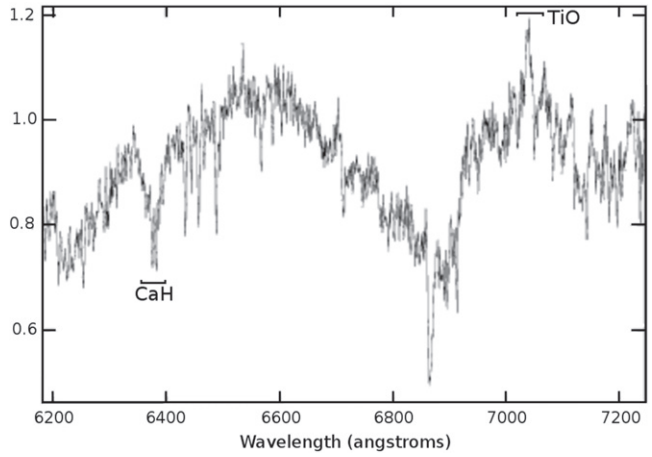

Figure 4. Extracted spectra for NLTT 52532 showing subdwarf characteristics, most apparent the weakness of the 7050 Å TiO band and strength of the 6380 Å CaH band. The *y*-axis is given in normalized arbitrary flux units.

Table 2
Full SOAR Spectroscopic Observation List

NLTT	m_v	ObsID	Companion?
2205	14.0	2014 Jul 14	Yes
7301	14.9	2014 Jul 14	Yes
7914	14.3	2014 Jul 14	Yes
9597	12.0	2014 Jul 14	···
9898	14.2	2014 Jul 14	···
10022	15.8	2014 Jul 14	···
10135	15.7	2014 Jul 14	···
33971	12.8	2014 Jul 14	···
37342	14.4	2014 Jul 14	Yes
37807	12.0	2014 Jul 14	···
40022	13.9	2014 Jul 14	···
40313	13.7	2014 Jul 14	···
41111	13.7	2014 Jul 14	···
44039	11.5	2014 Jul 14	···
44568	12.3	2014 Jul 14	···
49486	16.0	2014 Jul 14	Yes
50869	15.8	2014 Jul 14	···
52377	14.5	2014 Jul 14	Yes
52532	15.5	2014 Jul 14	Yes
53255	15.0	2014 Jul 14	Yes
55603	12.1	2014 Jul 14	Yes
56818	14.0	2014 Jul 14	Yes
57038	13.9	2014 Jul 14	Yes
58812	14.9	2014 Jul 14	Yes

right ascension and declination of >8 mas yr^{-1}. To locate possible fake companions, we use the high-proper motion survey LSPM (Lépine & Shara 2005), which is estimated over 99% complete in high galactic latitudes ($|b| > 15°$), where most of our targets lie. Out of approximately 21 million possible associations, we identified 12,451 pairs of stars, one of our subdwarf targets and an LSPM star, which have similar (below our dissociation threshold) proper-motion magnitude and direction. Known associated stars were removed from this sample. With our relatively small FOV and the large sky coverage of the LSPM, the probability of any of these pairs falling within our FOV is a remote 9.1×10^{-5}.

Table 3
Full Keck-AO Observation List

NLTT	m_v	ObsID	Companion?	ΔH
4817	11.4	2014 Aug 17	···	···
7914	14.3	2014 Aug 17	Yes	3.83
50869	15.8	2014 Aug 17	···	···
52377	14.5	2014 Aug 17	Yes	2.64
52532	15.5	2014 Aug 17	Yes	0.53
53255	15.0	2014 Aug 17	Yes	0.64
56818	14.0	2014 Aug 17	Yes	0.69

In addition, since our stars appear in relatively sparse stellar regions in the sky, well outside the Galactic disk, the probability of a background star appearing in a close radius to our observed star is low. Using the total number of known non-associated stars in our images, than at 95% confidence 7 of the 10 stars found within 2.″5 of any of our background stars are associated, with 9 of 10 being the most likely number of associated stars. The small number of probable unassociated background stars in our fields and the DSS proper-motion confirmations suggest a high-likelihood for true association for all of our companion stars.

4.2. Photometric Parallaxes

Very few subdwarfs in our sample have accurate parallax measurements. Only 43 of the targets have published parallaxes, most with significant measurement errors. To estimate the distances to our subdwarf targets, we employed an expression for $M_R = f(R - I)$ estimated by Siegel et al. (2002) using a color–magnitude diagram and the photometric measurements by Marshall (2007).

The polynomial fit found by Siegel for subdwarfs with measured parallaxes and an estimated mean [Fe/H] of −1.2, and with the Lutz & Kelker (1973) correction, is

$$M_R = 2.03 + 10 \times (R - I) - 2.21 \times (R - I)^2. \quad (3)$$

The color-absolute magnitude relation has an uncertainty of ∼0.3 mag. In all cases, the published parallax errors are much larger than photometric errors of <0.03 mag. The estimated distances for the primary stars in the subdwarf multiple systems are listed in Table 4.

5. DISCUSSION

5.1. Comparison to Main-sequence Dwarfs

With comparable sample size and spectrum types, the cool dwarf survey of Janson et al. (2012) is a useful metal-rich analog to this work. The study used the Lucky Imaging technique on a sample of 761 stars, sensitive to companion separations of 0.″08–6.″0. The most striking disparity between the two samples is the lack of low-contrast ($\Delta m_i \leqslant 2$), close ($\rho \leqslant 1''$) companions to the subdwarf stars, a regime heavily populated by solar-metallicity dwarf companions. This is clearly seen in a plot of the companion's magnitude difference versus angular separation for the two populations, as in Figure 9.

The dissimilarity between contrast ratios between dwarfs and subdwarfs is further illustrated in Figure 10. A two sample Kolmogrov–Smirnov test rejects the null hypothesis that the two populations are similar at a confidence of ∼2.8σ.

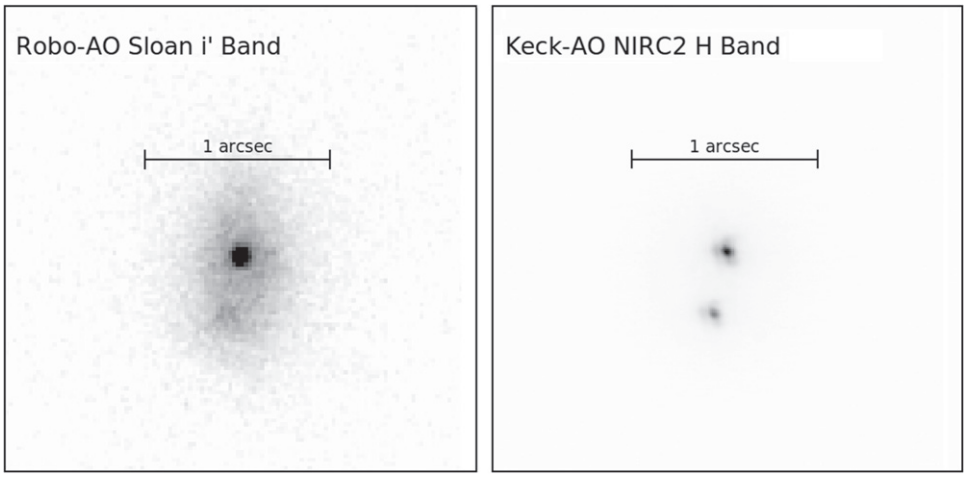

Figure 5. Keck-AO iamge confirming the Robo-AO companion to NLTT 52532. The exposure times are 120 s for the Robo-AO image and 90 s for the Keck image.

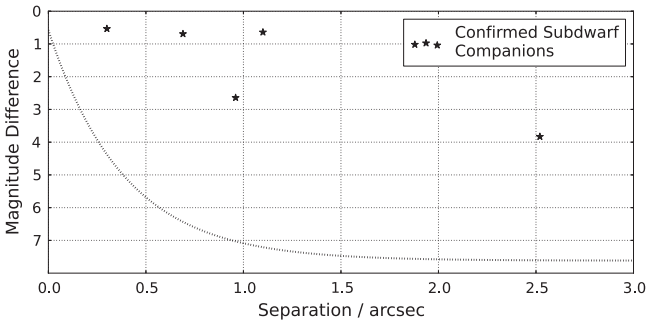

Figure 6. Plot of angular separation and *H*-band magnitude contrast for Keck confirmed Subdwarf companions. The detectable magnitude ratios for the Keck images is plotted, as described in Section 3.1.4.

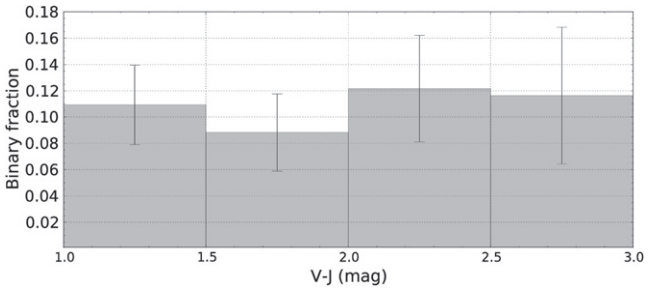

Figure 7. Binary fraction of the target subdwarfs binned by their $(V - J)$ color. The error bars were derived using binomial statistics.

The lack of close subdwarf companions has been noted previously by Jao et al. (2009) and by Abt (2008), but with significantly smaller samples. A direct comparison of orbital separations is biased by the distance variation in the two samples. With their rarity in the solar neighborhood, the subdwarf sample is overall approximately a factor of 4 further distant than the dwarf sample. If the populations were similar, this would result in a relative abundance of tight dwarf binaries, while the 6″ limit of the Janson et al. survey reduces the number of observed wide dwarf binaries. Attempts to pick out similar systems by relative distance or by orbital separation from the two surveys results in a small statistical sample. Nonetheless, the relative lack of close stars in the subdwarfs sample, as illustrated in Figure 11, and confirmed at high-confidence in our survey, warrants further investigation.

5.2. Binarity and Metallicity

The binary fraction we have found further confirms what has been suspected by past studies: that the binary fraction of subdwarfs is substantially lower than their dwarf cousins. The largest survey of cool subdwarfs, although limited by the low angular resolution of the SDSS, Zhang et al. (2013), find a multiplicity for type late K and M-subdwarfs of 2.41%, with an estimated lower bound of 10% when adjusting for survey incompleteness. This estimate and our work leave subdwarfs multiplicity rates approximately a factor of 2–4 lower than solar-metallicity stars of the same spectral types.

Historically, it has been a widely held view that metal-poor stars possess fewer stellar companions (Batten 1973; Latham 2004). A deficiency of eclipsing binaries was found in globular clusters by Kopal (1959), while Jaschek & Jaschek (1959) discovered a deficiency of spectroscopic binaries in a sample of high-velocity dwarfs. Abt & Willmarth (1987) used higher resolution CCD spectra to conclude that the frequency of spectroscopic binaries in high-velocity stars was half of metal-rich stars. Recently, however, this view has come under attack. Carney et al. (1994) used radial velocity measurements of 1464 stars, along with metallicity data (Carney et al. 1987), and found the difference in binary frequency of metal-rich and metal-poor stars to not be significant. Likewise, Grether & Lineweaver (2007) found a $\sim 2\sigma$ anti-correlation between metallicity and companion stars.

In recent years, the relationship between planetary systems and metallicity has also been explored. Fischer & Valenti (2005) found a positive correlation between planetary systems and the metallicity of the host star. This correlation has been reinforced to $\sim 4\sigma$ by Grether & Lineweaver (2007). Recently, Wang et al. (2014) found that planets in multiple-star systems occur 4.5 ± 3.2, 2.6 ± 1.0, and 1.7 ± 0.5 times less frequently when the companion star is separated by 10, 100, and 1000 AU, respectively.

The solution may lie in the differences between halo and thick disk stars. Latham et al. (2002) found no obvious difference between the binary fraction of the two populations;

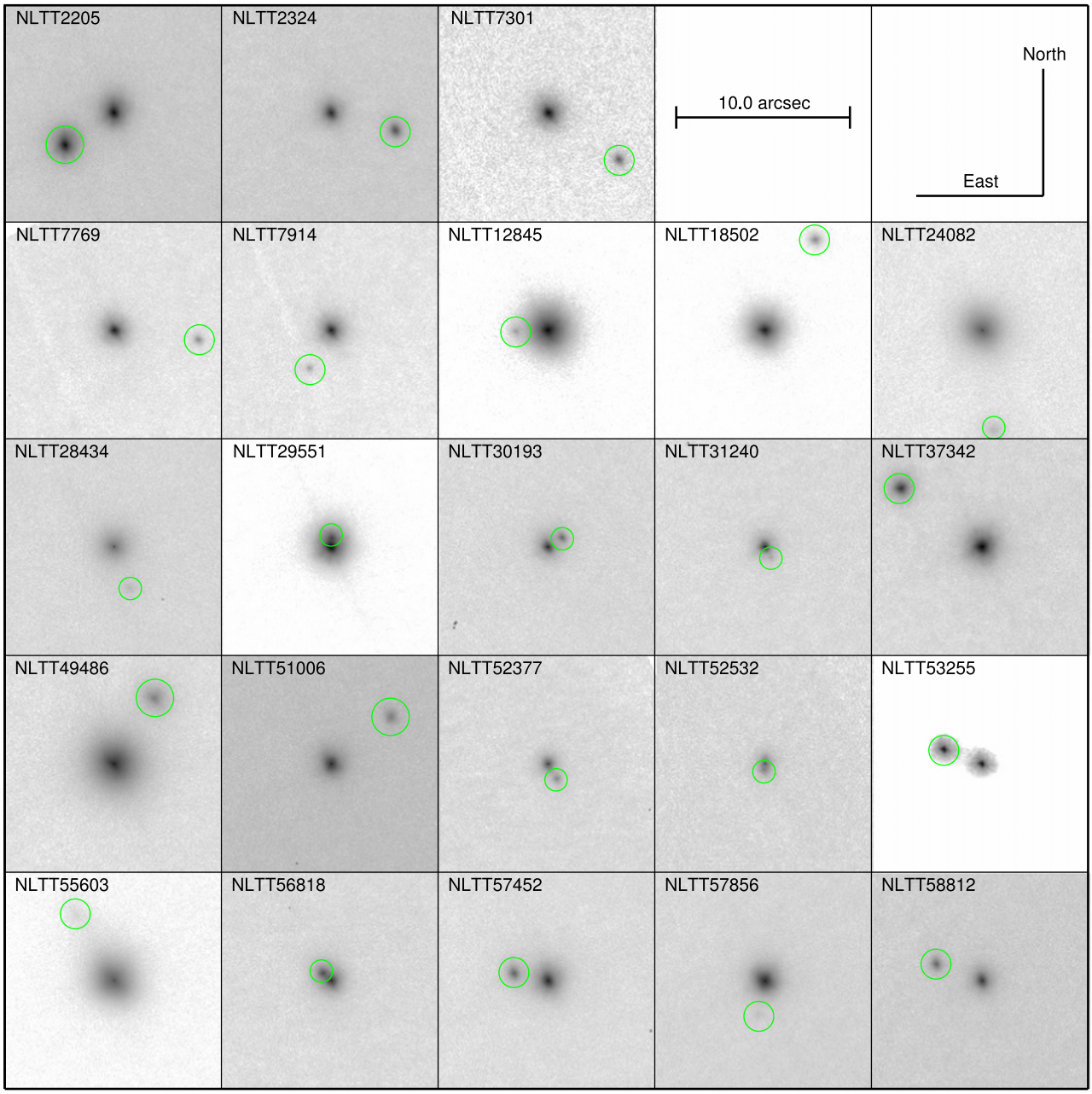

Figure 8. Color inverted, log-scale cutouts of the 23 multiple star systems with separations $<6''$ resolved with Robo-AO. The angular scale and orientation is similar for each cutout. The companions to NLTT 7914, 52377, 52532, and 56818 were confirmed with Keck II.

however Chiba & Beers (2000) found a 55% multiplicity rate for thick disk stars and 12% for halo stars. Grether & Lineweaver also find that the thick disk shows a ~4 times higher binary fraction than halo stars, further hypothesizing that the mixing of the populations is the explanation for the perceived anti-correlation of metallicity and binarity. Similarly, Bovy et al. (2012) use spectroscopic data to chart the disk thickness, finding, instead of a bi-modal separation of the thin and thick disks, a smooth, continuous distribution. This suggests the absence of a distinct thick disk in the Milky Way.

The large difference between the M-subdwarfs and thick-disk M-dwarfs, apparent in our work in this paper and Janson et al. (2012), seems to imply the two populations formed under different initial conditions. Star formation in less dense regions appears to lower binary rates. Köhler et al. (2006) found a factor 3–5 difference in binary fraction between the low-density Taurus star-forming region and the dense Orion cluster. It is also possible that, as forming earlier than solar-abundance stars, the metal-poor subdwarfs could have suffered more disruptive encounters with other stars and the Galactic tide (Kaib et al. 2013). These disturbances could separate companions with separations larger than a few AU, with the tighter, more highly bound systems being less affected (Sterzik & Durisen 1998; Abt 2008), a theory derived from *N*-body simulations (Aarseth & Hills 1972; Kroupa 1995; Jiang & Tremaine 2010). This, however, is contrary to our tentative result of a lack of close subdwarf companions, and the similar observations of Jao

Table 4
Multiple Subdwarf Systems Resolved Using Robo-AO and Previously Detected Systems

NLTT	Comp (NLTT)	m_v[a] (mag)	ObsID	Signif. (σ)	Δ i′ (mag)	ρ ($''$)	ρ (AU)	P.A. (deg.)	Dist (pc)	Prev Det?
2045AB	⋯	13.5	2013 Aug 15	⋯	⋯	⋯	⋯	⋯	183.3 ± 21.0	SB 9
2205AB	2206	13.9	2013 Aug 15	52	0.18	3.37	475.5 ± 54.3	123 ± 2	140.9 ± 16.1	L79
2324AB	2325	15.7	2013 Aug 16	19	1.16	3.84	138.8 ± 15.9	254 ± 2	36.1 ± 4.1	L79
2324AC	⋯	15.7	2013 Aug 16	16	4.14	23.48	847.8 ± 96.2	159 ± 2	36.1 ± 4.1	⋯
4817AB	4814	11.4	2012 Sep 3	65	4.30	24.59	3615 ± 413	218 ± 2	147 ± 16.8	S02
7301AB	7300	14.9	2012 Sep 3	30	2.48	4.87	105.7 ± 12.1	57 ± 2	21.7 ± 2.5	S02
7769AB	⋯	14.0	2012 Sep 3	8.2	3.34	4.84	1106 ± 126	121 ± 2	228.6 ± 26.2	⋯
7914AB	⋯	14.3	2012 Sep 3	39[b]	3.76	2.53[b]	424.4 ± 48.5	150 ± 2	167.6 ± 19.2	⋯
10536AB	10548	11.2	2013 Aug 15	⋯	⋯	185.7	30633 ± 3501	85.5	164.9 ± 18.9	S02
11015AB	11016	16.3	2013 Aug 16	42	0.94	9.24	1399 ± 160	57 ± 2	151.3 ± 17.3	S02
12845AB	⋯	10.6	2012 Oct 3	49	4.71	1.85	149.4 ± 17.1	92 ± 2	80.6 ± 9.2	⋯
15973AB	15974	9.3	2012 Oct 7	22	3.47	6.88	303.1 ± 34.6	227 ± 2	44 ± 5.0	S02
15973AC	⋯	9.3	2012 Oct 7	7.2	5.02	8.23	362.2 ± 41.1	217 ± 2	44 ± 5.0	⋯
17485AB	⋯	11.9	2012 Oct 10	⋯	⋯	⋯	⋯	⋯	191.3 ± 21.9	SB 9
18502AB	⋯	12.2	2013 Jan 19	25	3.18	5.95	1262 ± 144	331 ± 2	212.1 ± 24.3	⋯
18798AB	18799	14.5	2013 Jan 19	48	3.12	12.82	2270 ± 259	172 ± 2	177 ± 20.2	S02
19210AB	19207	11.2	2013 Jan 20	⋯	⋯	102.5	18468 ± 2110	285.4	180.2 ± 20.6	S02,SB 9
20691AB	⋯	9.6	2013 Jan 19	12	5.47	1.52	107.3 ± 12.3	93 ± 2	70.6 ± 8.1	SB 9
21370AB	⋯	13.7	2013 Jan 19	71	2.46	19.83	6603 ± 755	322 ± 2	332.9 ± 38.1	SB 9
24082AB	⋯	13.1	2013 Jan 19	4.8	4.46	5.81	1683 ± 192	187 ± 2	289.7 ± 33.1	⋯
24082AC	⋯	13.1	2013 Jan 19	3.8	4.17	12.00	3476 ± 397	267 ± 2	289.7 ± 33.1	⋯
25234AB	25233	13.2	2013 Jan 18	65	3.05	8.29	1175 ± 134	287 ± 2	141.7 ± 16.2	S02
28434AB	⋯	14.9	2013 Jan 17	2.2	2.46	2.54	652.9 ± 74.6	202 ± 2	256.7 ± 29.3	⋯
29551AB	⋯	11.5	2012 Sep 3	8.9	3.29	0.51	104.6 ± 12.0	355 ± 2	206.5 ± 23.6	⋯
29594AB	⋯	13.2	2013 Apr 22	⋯	⋯	38.10	12834 ± 1466	269	336.8 ± 38.5	L12
30193AB	⋯	14.6	2013 Apr 21	12	1.99	0.95	304.8 ± 34.8	304 ± 2	321.5 ± 36.7	⋯
30838AB	30837	12.5	2013 Apr 22	11	5.69	16.25	4436 ± 507	25 ± 2	273 ± 31.2	S02
31240AB	⋯	15.0	2013 Apr 21	13	3.86	10.32	3491 ± 399	157 ± 2	338.3 ± 38.7	⋯
31240AC	⋯	15.0	2013 Apr 21	5.1	4.16	0.74	251.2 ± 28.7	210 ± 2	338.3 ± 38.7	⋯
34051AB	⋯	13.5	2013 Jan 19	⋯	⋯	⋯	⋯	⋯	242.3 ± 27.7	SB 9
37342AB	37341	14.4	2013 Apr 22	49	1.37	5.75	123.4 ± 14.1	54 ± 2	21.4 ± 2.5	S02
45616AB	⋯	11.9	2012 Sep 3	125	2.59	28.31	4696 ± 536.8	113 ± 2	165.9 ± 19.0	SB 9
49486AB	49487	15.9	2012 Oct 4	9.3	1.48	4.51	390.3 ± 44.6	148 ± 2	86.4 ± 9.9	S02
49819AB	49821	14.0	2013 Aug 19	340	1.12	25.28	10263 ± 1173	84 ± 2	406 ± 46.4	S02
50759AB	⋯	15.9	2012 Sep 13	24	2.02	13.33	3544 ± 405	26 ± 2	265.8 ± 30.4	⋯
50759AC	50751	15.9	2012 Sep 13	⋯	⋯	297.7	79156 ± 9046	267.7	265.8 ± 30.4	S02
50869AB	⋯	15.8	2013 Aug 8	7.4	3.15	8.17	1707 ± 195	19 ± 2	209.0 ± 24.0	⋯
51006AB	⋯	14.0	2013 Aug 8	5.2	2.23	4.35	961.8 ± 109.9	76 ± 2	221.1 ± 25.3	⋯
52377AB	⋯	14.5	2012 Sep 4	568[b]	2.35	0.92[b]	561.3 ± 64.2	211 ± 2	585.3 ± 66.9	⋯
52532AB	⋯	15.5	2012 Sep 4	14[b]	2.60	0.30[b]	52.82 ± 6.0	168 ± 2	175 ± 20.0	⋯
52532AC	52538	15.5	2012 Sep 4	⋯	3.35	37.14	6536 ± 780	⋯	176 ± 21.0	L79
53255AB	⋯	15.0	2013 Aug 16	58[b]	0.75	1.07[b]	123.9 ± 14.2	68 ± 2	112.7 ± 12.9	⋯
53255AC	53254	15.0	2013 Aug 16	⋯	⋯	53.8	6063 ± 694	⋯	112.7 ± 12.9	L79
53274AB	⋯	11.8	2013 Aug 17	5.0	5.75	6.17	555.9 ± 63.5	153 ± 2	90.1 ± 10.3	⋯
55603AB	⋯	12.1	2013 Aug 18	2.6	3.54	4.45	886.9 ± 101.4	29 ± 2	199.2 ± 22.8	⋯
56818AB	⋯	14.0	2012 Sep 3	60[b]	2.04	0.63[b]	169.8 ± 19.4	44 ± 2	246.2 ± 28.1	⋯
57038AB	⋯	13.9	2013 Aug 16	210	0.19	8.14	2508 ± 286.7	335 ± 2	308.3 ± 35.2	⋯
57452AB	⋯	13.6	2013 Aug 16	14	1.91	1.98	474.5 ± 54.2	77 ± 2	234.9 ± 26.9	⋯
57856AB	⋯	13.2	2013 Aug 17	2.0	5.08	2.00	585.3 ± 66.9	169 ± 2	289.7 ± 33.1	⋯
58812AB	58813	15.0	2013 Aug 16	10	1.40	2.81	743.6 ± 85.0	69 ± 2	264.4 ± 30.2	⋯

Notes. References for previous detections are denoted using the following codes: Pourbaix et al. (2004) (SB 9), Luyten (1979) (L79), Saliom & Gould (2002) (S02), López et al. (2012) (L12).
[a] (Marshall 2007).
[b] From Keck follow-up, described in Section 3.4.

et al. (2009) and Abt (2008) that close subdwarf binaries are rare. This implies that metal-poor subdwarfs had shorter lifetimes in clusters than their younger, metal-rich cousins, either being ejected or formed in a disrupted cluster.

Another possible explanation is that a large number of low-metallicity stars in the Milky Way could have resulted from past mergers with satellite galaxies. Simulations from Abadi et al. (2006) predict that the early Galaxy underwent a period of active merging. From these mergers, the Galaxy would inherit large numbers of metal-poor stars. Meza et al. (2005) observe a group of metal-poor stars with angular momenta similar to the cluster ω Cen, long theorized to be the core of a

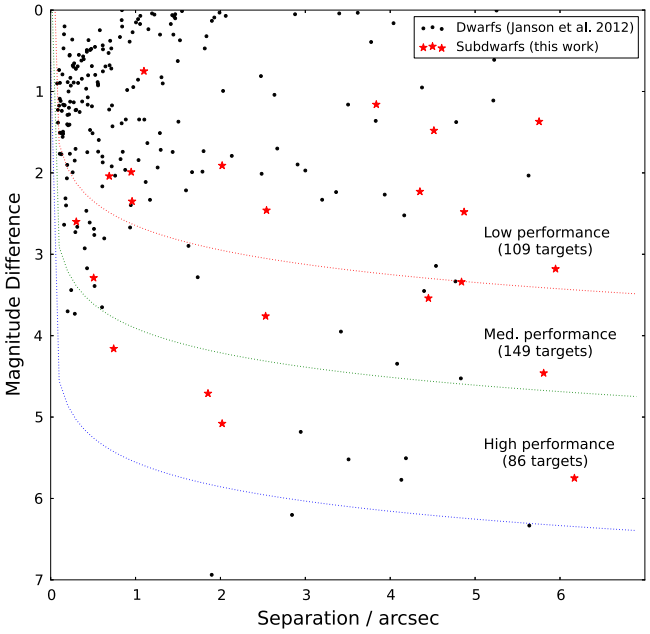

Figure 9. Comparison of the separation and the magnitude difference in the i-band between our subdwarf companions (<6″) and the dwarf companions found by Janson et al. (2012). The detectable magnitude ratios for our image performance groups are also plotted, with the number of observed subdwarf targets in each image performance group, as described in Section 3.1.4.

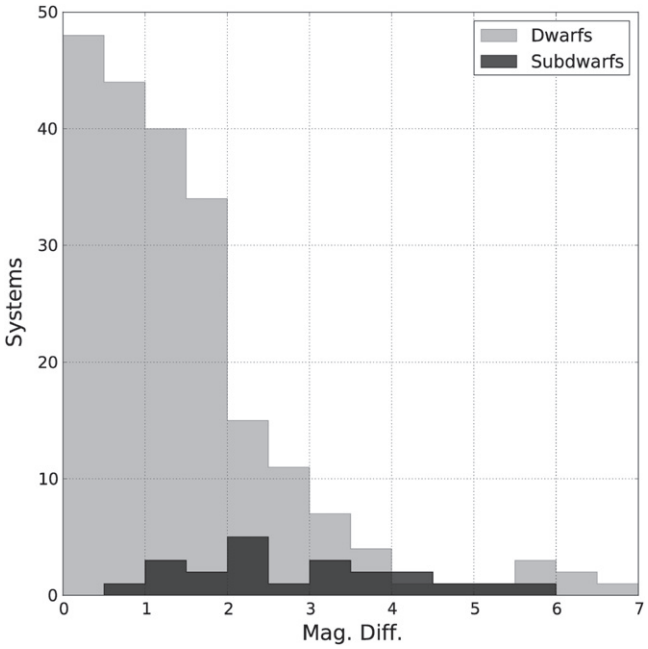

Figure 10. Histogram of the magnitude difference in the *i*-band between all our subdwarf companions and the dwarf companions found by Janson et al. (2012).

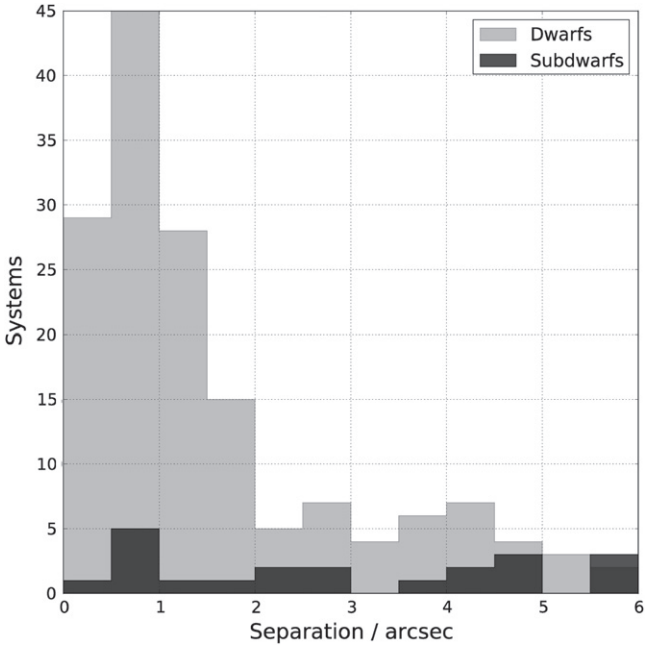

Figure 11. Histogram of the angular separations of our subdwarf companions and the dwarf companions found by Janson et al. (2012). Only systems resolvable in both surveys were plotted ($0\farcs15 < \rho < 6\farcs0$).

dwarf galaxy that merged with the Milky Way. The environment of these foreign galaxies is unknown, so star formation could be quite different than our own Galaxy. It is also possible that during the merger multiple close stellar encounters and perturbations could alter their primordial binary properties.

6. CONCLUSIONS

In the largest high-resolution binary survey of cool subdwarfs, we observed 344 stars with the Robo-AO robotic laser adaptive optics system, sensitive to companions at $\rho \geqslant 0\farcs15$ and $\Delta m_i \leqslant 6$. Of those targets, we observed 16 new multiple systems and five new companions to already known binary systems. When including previously recorded multiple systems, this implies a multiplicity rate for cool subdwarfs of 12.5 $\pm$ 1.9% and a triplet fraction of 2.0 $\pm$ 0.8%. This is significantly lower than the observed cool subdwarf binarity of 26 $\pm$ 6% by Jao et al. (2009) and in agreement with the completeness adjusted estimate of >10% of Zhang et al. (2013). When comparing our results to similar surveys of non-subdwarf binarity, we note a $\sim$2.8σ difference in relative magnitude differences between companions. An apparent lack of close binaries is noted, as has been previously observed in the literature. The high efficiency of Robo-AO makes large, high-angular resolution surveys practical and will in the future continue to put tighter constraints on the properties of stellar populations.

We would like to acknowledge the anonymous referee for careful analysis of our paper and the comments that have improved it. The Robo-AO system is supported by collaborating partner institutions, the California Institute of Technology and the Inter-University Centre for Astronomy and Astrophysics, and by the National Science Foundation under Grant Nos. AST-0906060, AST-0960343, and AST-1207891, by the Mount Cuba Astronomical Foundation, and by a gift from Samuel Oschin. We are grateful to the Palomar Observatory staff for their ongoing support of Robo-AO on the 60 inch telescope, particularly S. Kunsman, M. Doyle, J. Henning, R. Walters, G. Van Idsinga, B. Baker, K. Dunscombe, and D. Roderick. The SOAR telescope is operated by the Association of Universities for Research in Astronomy, Inc., under a cooperative agreement between the CNPq, Brazil, the National Observatory for Optical Astronomy (NOAO), the University of North Carolina, and Michigan State University, USA. We also

Table A1
Full Robo-AO Observation List

NLTT	m_v	ObsID	Obs. Qual	Companion?
69	15.2	2012 Oct 10	Low	⋯
193	15.5	2013 Aug 15	Medium	⋯
341	12.1	2012 Oct 10	High	⋯
361	15.4	2013 Aug 17	Low	⋯
496	15.8	2012 Sep 04	Medium	⋯
660	15.7	2012 Sep 03	Low	⋯
812	12.8	2012 Sep 03	High	⋯
933	15.5	2013 Aug 16	Low	⋯
1020	15.3	2013 Aug 15	Medium	⋯
1059	13.8	2012 Sep 04	Medium	⋯
1231	11.9	2013 Aug 16	High	⋯
1509	15.8	2013 Aug 16	Low	⋯
1575	16.2	2012 Sep 03	Low	⋯
1635	13.2	2012 Sep 03	High	⋯
1684	15.1	2012 Sep 13	Low	⋯
1815	15.5	2012 Sep 04	Low	⋯
1870	13.9	2012 Sep 03	Medium	⋯
2045	13.5	2013 Aug 15	Medium	Yes
2107	15.5	2012 Sep 04	Low	⋯
2205	14.0	2013 Aug 15	Medium	Yes
2324	15.7	2013 Aug 16	Medium	Yes
2868	13.5	2013 Aug 16	Medium	⋯
2953	15.9	2012 Sep 04	Low	⋯
2966	15.6	2012 Sep 04	Medium	⋯
3035	15.9	2012 Sep 04	Low	⋯
3965	16.1	2013 Aug 16	Medium	⋯
4245	15.6	2013 Aug 15	Low	⋯
4447	15.9	2012 Sep 03	Low	⋯
4817	11.4	2012 Sep 03	High	Yes
4838	15.4	2012 Sep 03	Low	⋯
5022	13.9	2012 Sep 03	Medium	⋯
5192	14.3	2012 Sep 03	Medium	⋯
5289	15.6	2012 Sep 03	Low	⋯
6519	14.8	2012 Sep 03	Medium	⋯
6582	15.7	2013 Aug 17	Low	⋯
6614	15.7	2012 Sep 03	Medium	⋯
6816	16.1	2013 Aug 15	Low	⋯
6856	16.1	2012 Sep 03	Low	⋯
6863	15.3	2013 Aug 17	Low	⋯
7078	14.4	2012 Sep 03	Medium	⋯
7207	14.5	2013 Aug 15	Medium	⋯
7299	11.5	2013 Aug 16	High	⋯
7301	14.9	2012 Sep 03	High	Yes
7415	9.1	2012 Sep 03	High	⋯
7417	11.6	2013 Aug 15	High	⋯
7467	15.9	2012 Sep 13	Low	⋯
7596	16.2	2013 Aug 17	Low	⋯
7654	16.1	2013 Aug 16	Medium	⋯
7769	14.0	2012 Sep 03	Medium	Yes
7914	14.3	2012 Sep 03	Medium	Yes
8034	11.8	2012 Sep 03	High	⋯
8227	10.5	2013 Aug 17	High	⋯
8342	14.9	2012 Sep 03	Medium	⋯
8405	15.8	2012 Sep 03	Medium	⋯
8507	13.9	2012 Sep 03	Medium	⋯
8783	11.5	2012 Sep 03	High	⋯
8866	15.8	2013 Aug 16	Low	⋯
9523	15.4	2013 Aug 15	Low	⋯
9550	15.5	2013 Aug 19	Low	⋯
9578	10.5	2013 Aug 15	High	⋯
9597	12.0	2012 Sep 13	High	⋯
9622	14.3	2012 Sep 04	Medium	⋯
9648	14.9	2012 Sep 04	Medium	⋯

Table A1
(Continued)

NLTT	m_v	ObsID	Obs. Qual	Companion?
9653	15.6	2013 Aug 16	Low	⋯
9727	15.8	2013 Aug 15	Medium	⋯
9734	15.0	2012 Sep 04	Medium	⋯
9799	15.4	2012 Sep 13	Low	⋯
9848	16.6	2013 Aug 19	Low	⋯
9898	14.2	2013 Aug 19	Low	⋯
9938	16.2	2013 Aug 15	Low	⋯
10018	15.4	2013 Aug 17	Low	⋯
10022	15.8	2013 Aug 16	Medium	⋯
10135	15.7	2012 Sep 04	Low	⋯
10176	15.8	2013 Aug 20	Low	⋯
10243	14.1	2012 Sep 04	Medium	⋯
10401	14.6	2013 Aug 18	Low	⋯
10517	14.5	2012 Sep 04	Medium	⋯
10536	11.2	2013 Aug 15	High	Yes
10548	15.9	2013 Aug 15	Low	⋯
10850	10.7	2012 Sep 04	High	⋯
10883	15.9	2012 Sep 04	Low	⋯
11007	12.2	2013 Aug 21	High	⋯
11010	14.1	2012 Sep 04	Medium	⋯
11015	16.3	2013 Aug 16	Low	Yes
11032	14.2	2012 Sep 04	Medium	⋯
11068	15.4	2013 Aug 21	Low	⋯
11938	14.3	2012 Sep 04	Medium	⋯
12017	12.3	2013 Aug 17	High	⋯
12026	15.8	2013 Aug 18	Low	⋯
12044	15.8	2012 Sep 13	Low	⋯
12227	14.2	2013 Aug 18	Medium	⋯
12350	12.1	2013 Aug 18	Medium	⋯
12489	14.6	2012 Oct 10	Low	⋯
12537	14.5	2013 Aug 21	Medium	⋯
12704	15.4	2012 Oct 10	Low	⋯
12769	14.1	2013 Aug 18	Medium	⋯
12829	14.6	2012 Oct 03	Medium	⋯
12845	10.6	2012 Oct 03	High	Yes
12856	10.8	2013 Aug 18	High	⋯
12876	15.6	2012 Oct 03	Low	⋯
12923	15.2	2013 Aug 18	Low	⋯
13022	15.9	2012 Oct 03	Low	⋯
13344	13.8	2012 Oct 03	Medium	⋯
13368	15.5	2012 Oct 03	Low	⋯
13402	14.7	2012 Oct 03	Low	⋯
13469	15.1	2013 Aug 18	Low	⋯
13470	13.8	2012 Oct 03	Medium	⋯
13641	12.9	2012 Oct 06	High	⋯
13660	12.4	2012 Oct 03	High	⋯
13694	15.4	2013 Aug 20	Medium	⋯
13706	14.5	2012 Oct 03	Low	⋯
13770	12.4	2012 Oct 03	High	⋯
13811	13.4	2012 Oct 03	Medium	⋯
13920	14.4	2013 Aug 20	Medium	⋯
13940	14.4	2012 Oct 05	Medium	⋯
14091	13.9	2012 Oct 05	Medium	⋯
14131	13.4	2012 Oct 03	Medium	⋯
14169	13.4	2012 Oct 05	Medium	⋯
14197	12.4	2012 Oct 04	Low	⋯
14391	13.5	2012 Oct 04	Low	⋯
14450	14.7	2012 Oct 04	Low	⋯
14549	14.5	2012 Oct 10	Low	⋯
14822	12.7	2012 Oct 03	Medium	⋯
14864	14.3	2012 Oct 07	Low	⋯
15039	14.8	2012 Oct 10	Low	⋯
15183	12.6	2012 Oct 07	Medium	⋯
15218	12.3	2012 Oct 06	High	⋯

Table A1
(Continued)

NLTT	m_v	ObsID	Obs. Qual	Companion?
15973	9.3	2012 Oct 07	High	Yes
15974	13.8	2012 Oct 07	High	⋯
16030	13.9	2012 Oct 07	Low	⋯
16185	14.4	2012 Oct 10	Low	⋯
16242	10.6	2012 Oct 06	Medium	⋯
16579	12.3	2012 Oct 09	High	⋯
16606	12.3	2012 Oct 10	High	⋯
16849	15.3	2012 Oct 10	Low	⋯
16869	13.2	2013 Jan 20	High	⋯
16986	15.8	2013 Jan 20	Low	⋯
17039	12.9	2012 Oct 10	Medium	⋯
17485	11.9	2012 Oct 10	High	Yes
17680	13.6	2013 Jan 20	Medium	⋯
17786	12.0	2013 Jan 20	High	⋯
17872	10.7	2013 Jan 20	High	⋯
18019	13.3	2012 Oct 10	Medium	⋯
18131	14.4	2013 Jan 20	Medium	⋯
18424	12.7	2013 Jan 18	High	⋯
18463	13.8	2013 Jan 20	High	⋯
18502	12.2	2013 Jan 19	High	Yes
18731	13.1	2013 Jan 19	High	⋯
18798	14.5	2013 Jan 19	High	Yes
18799	11.0	2013 Jan 19	High	⋯
19037	14.9	2013 Jan 20	Medium	⋯
19210	11.2	2013 Jan 20	High	Yes
19301	14.7	2013 Jan 19	Low	⋯
19570	14.4	2013 Apr 22	Medium	⋯
19614	15.7	2013 Apr 22	Medium	⋯
19643	11.9	2013 Jan 19	High	⋯
19824	14.6	2013 Jan 19	Medium	⋯
20252	14.9	2013 Apr 22	Medium	⋯
20288	14.9	2013 Apr 22	Medium	⋯
20392	13.8	2013 Jan 22	Low	⋯
20476	13.2	2013 Apr 22	High	⋯
20492	13.3	2013 Jan 19	High	⋯
20684	12.0	2013 Jan 19	High	⋯
20691	9.6	2013 Jan 19	High	Yes
20768	14.0	2013 Jan 19	Medium	⋯
21039	14.0	2013 Jan 19	Medium	⋯
21112	15.3	2013 Apr 22	Medium	⋯
21133	12.7	2013 Jan 19	Medium	⋯
21341	14.3	2013 Jan 19	Low	⋯
21370	13.7	2013 Jan 19	Medium	Yes
21449	12.6	2013 Apr 22	High	⋯
21601	14.6	2013 Apr 22	Medium	⋯
22026	12.6	2013 Apr 22	High	⋯
22053	12.1	2013 Jan 19	High	⋯
22520	10.8	2013 Jan 19	High	⋯
22752	13.9	2013 Jan 19	Medium	⋯
22945	13.2	2013 Apr 22	Medium	⋯
23894	14.6	2013 Jan 18	Low	⋯
24006	15.5	2013 Apr 22	Medium	⋯
24082	13.1	2013 Jan 19	Medium	Yes
24353	13.2	2013 Jan 18	Medium	⋯
24371	14.2	2013 Jan 18	Low	⋯
24718	13.1	2013 Jan 18	Medium	⋯
24984	12.5	2013 Apr 21	High	⋯
25006	14.1	2013 Apr 21	Medium	⋯
25177	12.2	2013 Apr 22	High	⋯
25190	13.9	2013 Jan 18	Low	⋯
25234	13.2	2013 Jan 18	Medium	Yes
25475	13.9	2013 Apr 21	Medium	⋯
25776	13.8	2013 Apr 22	Medium	⋯
25909	13.5	2013 Apr 22	High	⋯

Table A1
(Continued)

NLTT	m_v	ObsID	Obs. Qual	Companion?
25970	14.9	2013 Jan 18	Low	⋯
26232	14.4	2013 Jan 18	Low	⋯
26482	12.5	2013 Jan 18	Medium	⋯
26503	14.2	2013 Apr 21	Medium	⋯
26532	14.8	2013 Jan 18	Low	⋯
26565	14.8	2013 Jan 18	Low	⋯
26588	13.6	2013 Apr 21	High	⋯
26677	13.5	2013 Jan 18	Low	⋯
27436	13.0	2013 Jan 18	Medium	⋯
27763	13.6	2013 Jan 18	Medium	⋯
27767	14.7	2013 Apr 21	Medium	⋯
28199	13.2	2013 Jan 18	Medium	⋯
28304	13.3	2013 Apr 22	Medium	⋯
28434	14.9	2013 Jan 17	Low	Yes
29023	13.0	2013 Jan 18	Medium	⋯
29064	14.0	2013 Apr 21	Medium	⋯
29256	14.7	2013 Jan 18	Low	⋯
29442	14.4	2013 Jan 18	Low	⋯
29551	11.5	2013 Apr 21	High	Yes
29594	13.2	2013 Apr 22	High	Yes
29933	10.2	2013 Apr 22	High	⋯
30128	13.1	2013 Apr 21	High	⋯
30193	14.6	2013 Apr 21	Medium	Yes
30462	12.8	2013 Jan 18	Medium	⋯
30636	14.8	2013 Jan 18	Low	⋯
30824	14.6	2013 Jan 17	Low	⋯
30838	12.5	2013 Apr 22	High	Yes
31146	12.0	2013 Apr 21	High	⋯
31155	13.6	2013 Jan 18	Medium	⋯
31240	15.0	2013 Apr 21	Medium	Yes
31965	14.2	2013 Jan 19	Medium	⋯
32316	11.3	2013 Apr 22	High	⋯
32392	14.6	2013 Jan 19	Medium	⋯
32562	14.3	2013 Jan 17	Low	⋯
32648	12.8	2013 Jan 18	Medium	⋯
32917	13.8	2013 Apr 22	Medium	⋯
32995	13.4	2013 Apr 22	High	⋯
33104	14.0	2013 Jan 18	Low	⋯
33156	14.2	2013 Apr 22	Medium	⋯
33371	12.8	2013 Jan 17	Medium	⋯
33971	12.8	2013 Jan 18	Medium	⋯
34051	13.5	2013 Jan 19	Low	Yes
34628	11.9	2013 Apr 21	High	⋯
35068	13.2	2013 Jan 18	Medium	⋯
35318	13.4	2013 Apr 21	High	⋯
36020	14.2	2013 Apr 22	Medium	⋯
37342	14.4	2013 Apr 22	High	Yes
37684	13.3	2013 Apr 22	High	⋯
37807	12.0	2013 Apr 22	High	⋯
39378	13.5	2013 Apr 22	High	⋯
39721	13.6	2013 Apr 22	High	⋯
40022	13.9	2013 Apr 22	Medium	⋯
40313	13.7	2013 Apr 22	High	⋯
41111	13.7	2013 Apr 22	Medium	⋯
44039	11.5	2012 Sep 14	High	⋯
44233	15.2	2012 Sep 04	Low	⋯
44568	12.3	2012 Sep 04	High	⋯
44639	11.8	2012 Sep 04	High	⋯
44769	15.2	2013 Apr 21	Medium	⋯
45609	12.5	2012 Sep 04	High	⋯
45616	11.9	2012 Sep 04	High	Yes
47543	9.2	2012 Oct 05	Medium	⋯
48011	14.7	2012 Oct 05	High	⋯
48056	13.7	2012 Oct 07	Low	⋯

Table A1
(Continued)

NLTT	m_v	ObsID	Obs. Qual	Companion?
48391	15.2	2012 Oct 05	Medium	⋯
48592	12.2	2012 Oct 04	Medium	⋯
48866	12.7	2012 Oct 04	Medium	⋯
49486	16.0	2012 Oct 04	Medium	Yes
49487	12.3	2012 Oct 04	Medium	⋯
49488	14.9	2013 Aug 19	Medium	⋯
49618	12.2	2012 Oct 04	Medium	⋯
49726	15.9	2013 Aug 19	Low	⋯
49749	14.8	2012 Oct 03	Medium	⋯
49819	14.0	2013 Aug 19	High	Yes
49821	12.8	2013 Aug 19	High	⋯
49897	15.8	2012 Oct 04	Low	⋯
50257	13.8	2013 Aug 18	Low	⋯
50376	13.9	2012 Sep 13	Medium	⋯
50556	15.7	2012 Sep 13	Low	⋯
50759	15.9	2012 Sep 13	Low	Yes
50869	15.8	2013 Aug 19	Low	⋯
50911	11.6	2012 Sep 13	High	⋯
51006	14.1	2013 Aug 19	Medium	Yes
51153	15.1	2012 Sep 13	Low	⋯
51740	15.3	2012 Sep 13	Low	⋯
51754	15.0	2012 Sep 13	Low	⋯
51824	11.9	2013 Aug 18	Medium	⋯
51856	13.4	2012 Sep 04	Medium	⋯
52089	14.9	2012 Sep 04	Medium	⋯
52377	14.5	2012 Sep 04	Medium	Yes
52532	15.5	2012 Sep 04	Low	Yes
52573	15.3	2013 Aug 18	Low	⋯
52666	15.0	2013 Aug 19	Low	⋯
52816	15.7	2012 Sep 13	Low	⋯
52894	16.0	2012 Sep 13	Low	⋯
53190	15.4	2013 Aug 16	Medium	⋯
53254	14.7	2013 Aug 16	Medium	⋯
53255	15.0	2013 Aug 16	Medium	Yes
53274	11.9	2013 Aug 17	High	Yes
53316	15.4	2012 Sep 13	Low	⋯
53346	13.8	2013 Aug 17	Medium	⋯
53480	12.6	2013 Aug 17	High	⋯
53702	15.3	2012 Sep 13	Medium	⋯
53707	12.1	2013 Aug 18	Medium	⋯
53781	13.8	2013 Aug 17	Medium	⋯
53801	11.8	2012 Sep 13	High	⋯
53823	13.8	2013 Aug 18	Low	⋯
54027	13.3	2013 Aug 19	Medium	⋯
54088	14.1	2013 Aug 18	Low	⋯
54168	13.4	2013 Aug 17	Medium	⋯
54184	14.0	2013 Aug 17	Medium	⋯
54349	14.4	2012 Sep 13	Medium	⋯
54450	15.6	2013 Aug 16	Low	⋯
54578	15.8	2013 Aug 18	Low	⋯
54608	16.0	2013 Aug 16	Low	⋯
54620	15.2	2013 Aug 17	Medium	⋯
54699	15.1	2012 Sep 13	Low	⋯
54710	15.2	2012 Sep 13	Low	⋯
54730	11.5	2012 Sep 13	High	⋯
55411	15.9	2013 Aug 16	Low	⋯
55603	12.1	2013 Aug 18	Medium	Yes
55732	13.4	2013 Aug 17	Medium	⋯
55733	14.5	2012 Sep 03	Medium	⋯
55942	13.5	2013 Aug 16	Medium	⋯
56002	14.4	2012 Sep 03	Medium	⋯
56290	12.6	2013 Aug 16	High	⋯
56420	15.6	2012 Sep 03	Low	⋯

Table A1
(Continued)

NLTT	m_v	ObsID	Obs. Qual	Companion?
56533	15.9	2013 Aug 16	Low	⋯
56534	12.7	2013 Aug 17	High	⋯
56774	12.9	2013 Aug 18	Low	⋯
56817	16.1	2013 Aug 17	Low	⋯
56818	14.0	2012 Sep 03	Medium	Yes
56855	13.7	2013 Aug 16	Medium	⋯
57038	13.9	2013 Aug 16	Medium	Yes
57214	15.8	2013 Aug 16	Low	⋯
57452	13.6	2013 Aug 16	Medium	Yes
57546	16.2	2013 Aug 17	Low	⋯
57564	10.6	2013 Aug 17	High	⋯
57630	15.0	2013 Aug 16	Medium	⋯
57631	13.5	2013 Aug 17	Medium	⋯
57647	14.7	2013 Aug 17	Medium	⋯
57741	14.2	2013 Aug 17	Medium	⋯
57744	16.1	2013 Aug 17	Low	⋯
57781	10.1	2013 Aug 16	High	⋯
57832	15.2	2012 Sep 03	Medium	⋯
57851	15.2	2012 Sep 03	Medium	⋯
57856	13.2	2013 Aug 17	Medium	Yes
58071	13.1	2012 Sep 03	Medium	⋯
58141	15.8	2013 Aug 16	Low	⋯
58403	15.2	2013 Aug 16	Low	⋯
58522	15.0	2013 Aug 17	Medium	⋯
58555	15.1	2012 Sep 03	Medium	⋯
58812	14.9	2013 Aug 16	Medium	Yes

thank the SOAR operators, notably Sergio Pizarro. We recognize and acknowledge the very significant cultural role and reverence that the summit of Maunakea has always had within the indigenous Hawaiian community. We are most fortunate to have the opportunity to conduct observations from this mountain. C.B. acknowledges support from the Alfred P. Sloan Foundation. This research has made use of the SIMBAD database, operated by Centre des Données Stellaires (Strasbourg, France), and bibliographic references from the Astrophysics Data System maintained by SAO/NASA.

Facilities: PO:1.5m (Robo-AO), Keck:II (NIRC2-LGS), SOAR (Goodman)

APPENDIX

In Table A1, we list our Robo-AO observed subdwarfs, including date the target was observed, observation quality as described in Section 3.1.4, and the presence of detected companions.

REFERENCES

Aarseth, S. L., & Hills, J. G. 1972, A&A, 21, 255
Abadi, M. G., Navarro, J. F., & Stenmetz, M. 2006, MNRAS, 365, 747
Abell, G. O. 1959, ASPL, 8, 121
Abt, H. A. 2008, AJ, 135, 722
Abt, H. A., & Willmarth, D. W. 1987, ApJ, 318, 786
Adams, W. S. 1915, AJ, 42, 187
Baranec, C., Riddle, R., Law, N. M., et al. 2013, J. Visualized Exp., 72, e50021
Baranec, C., Riddle, R., Law, N. M., et al. 2014, ApJL, 790, L8
Basu, S., & Vorobyov, E. I. 2012, ApJ, 750, 30
Batten, A. H. 1973, Binary and Multiple Systems of Stars (Oxford: Pergamon)
Bourke, T. L., Myers, P. C., Evans, N. J., II, et al. 2006, ApJL, 649, L37
Bovy, J., Rix, H.-W., & Hogg, D. W. 2012, ApJ, 751, 131

Burgasser, A. J., Kirkpatrick, J. D., Reid, I. N., et al. 2003, ApJ, 586, 512
Carney, B. W., Laird, J. B., Latham, D. W., & Kurucz, R. L. 1987, AJ, 94, 1066
Carney, B. W., Latham, D. W., Laird, J. B., & Anguilar, L. A. 1994, AJ, 107, 2240
Chabrier, G., Baraffe, I., Allard, F., & Hauschildt, P. 2000, ApJ, 542, 464
Chanamé, J., & Gould, A. 2004, ApJ, 601, 289
Chiba, M., & Beers, T. C. 2000, ApJ, 119, 2843
Clemens, J. C., Crain, J. A., & Anderson, R. 2004, Proc. SPIE, 5492, 331
Ducati, J. R., Bevilacqua, C. M., Rembold, S. B., & Ribeiro, D. 2001, ApJ, 558, 309
Duquennoy, A., & Mayor, M. 1991, A&A, 248, 485
Fischer, D. A., & Marcy, G. 1992, ApJ, 396, 178
Fischer, D. A., & Valenti, J. 2005, ApJ, 622, 1102
Fruchter, A. S., & Hook, R. N. 2002, PASP, 114, 144
Gizis, J. E. 1997, AJ, 113, 806
Gizis, J., & Reid, I. N. 2000, PASP, 112, 610
Goodwin, S. P., Kroupa, P., Goodman, A., & Burkert, A. 2007, in Protostars and Planets V, ed. B. Reipurth, D. Jewitt, & K. Kiel (Tucson, AZ: Univ. Arizona Press), 133
Goodwin, S. P., & Whitworth, A. 2007, A&A, 466, 943
Gould, A. 2003, ApJ, 583, 765
Gould, A., & Salim, S. 2003, ApJ, 582, 1001
Grether, D., & Lineweaver, C. H. 2007, ApJ, 669, 1220
Janson, M., Bergfors, C., Brandner, W., et al. 2014, ApJS, 214, 17
Janson, M., Hormuth, F., Bergfors, C., et al. 2012, ApJ, 754, 44
Jao, W.-C., Mason, B. D., Hartkopf, W. I., et al. 2009, AJ, 137, 3800
Jaschek, C., & Jaschek, M. 1959, Zt. F. Ap., 48, 263
Jiang, Y.-F., & Tremaine, S. 2010, MNRAS, 401, 977
Kaib, N. A., Raymond, S. N., & Duncan, N. 2013, Natur, 493, 381
Kaltenegger, L., & Traub, W. A. 2009, ApJ, 609, 519
Köhler, R., Petr-Gotzens, M. G., McCaughrean, M. J., et al. 2006, A&A, 458, 461
Kopal, Z. 1959, Close Binary Systems (New York: Wiley)
Kroupa, P. 1995, MNRAS, 277, 1491
Kuiper, G. P. 1939, ApJ, 89, 548
Lafrenière, D., Marois, C., Doyon, R., Nadeau, D., & Artigau, É 2007, ApJ, 660, 770
Latham, D. W. 2004, in ASP Conf. Ser. 318, Spectroscopically and Spatially Resolving the Components of the Close Binary Stars, ed. R. W. Hilditch, H. Hensberge, & K. Pavlovski (San Francisco, CA: ASP), 276
Latham, D. W., Stefanik, R. P., Torres, G., et al. 2002, ApJ, 124, 1144
Law, N. M., Hodgkin, S. T., & Mackay, C. D. 2006, MNRAS, 368, 1917
Law, N. M., Mackay, C. D., Dekany, R. G., et al. 2009, ApJ, 692, 924
Law, N. M., Morton, T., Baranec, C., et al. 2014, ApJ, 791, 35
Lépine, S., Rich, R. M., & Shara, M. M. 2007, ApJ, 669, 1235
Lépine, S., & Shara, M. 2005, AJ, 129, 1483
Lodieu, N., Zapatero Osorio, M. R., & Martín, E. L. 2009, A&A, 499, 729
López, C. E., Calandra, F., Chalela, M., et al. 2012, JDSO, 8, 78
Lutz, T. E., & Kelker, D. H. 1973, PASP, 85, 573
Luyten, W. J. 1979, New Luyten Catalogue of Stars with Proper Motions Larger than Two-Tenths of an Arcsecond (Minneapolis, MN: Univ. Minnesota Press)
Luyten, W. J., & Hughes, H. S. 1980, Proper-Motion Survey with the Forty-Eight Inch Schmidt Telescope LV First Supplement to the NLTT Catalogue (Minneapolis, MN: Univ. Minnesota Press)
Marshall, J. L. 2007, AJ, 134, 778
Marshall, J. L. 2008, AJ, 135, 1000
Meza, A., Navarro, J. F., Abadi, M. G., & Stenmetz, M. 2005, MNRAS, 359, 93
Monteiro, H., Jao, W.-C., Henry, T., et al. 2006, ApJ, 638, 446
Peter, D., Feldt, M., Henning, T., & Hormuth, F. 2012, A&A, 538, 74
Pourbaix, D., Tokovinin, A. A., Batten, A. H., et al. 2004, A&A, 424, 727
Raghavan, D., McAlister, H. A., Henry, T. J., et al. 2010, ApJS, 190, 1
Reid, I. N., Brewer, C., Brucato, R. J., et al. 1991, PASP, 103, 661
Reid, I. N., & Hawley, S. L. 2005, New Light on Dark Stars: Red Dwarfs, Low-Mass Stars, Brown Dwarfs (1st ed.; Chichester, UK: Praxis)
Riaz, B., Gizis., J., & Samaddar, D. 2008, ApJ, 672, 1153
Riddle, R. L., Burse, M. P., Law, N. M., et al. 2012, Proc. SPIE, 8447, 84472O
Salim, S., & Gould, A. 2002, ApJL, 575, L83
Siegel, M. H., Majewski, S. R., Reid, I. N., & Thompson, I. B. 2002, ApJ, 578, 151
Sterzik, M. F., & Durisen, R. H. 1998, A&A, 339, 95
Thies, I., & Kroupa, P. 2007, ApJ, 671, 767
Sandage, A., & Eggen, O. 1959, MNRAS, 119, 278
van Dam, M., Bouchez, A., Le Mignant, D., et al. 2006, PASP, 118, 310
Wang, J., Fischer, D. A., Xie, J.-W., & Ciardi, D. R. 2014, ApJ, 792, 111
Wizinowich, P., Le Mignant, D., Bouchez, A., et al. 2006, PASP, 118, 297
York, D. G., Adelman, J., Anderson, J. E., et al. 2000, AJ, 120, 1579
Zhang, Z. H., Pinfield, D. J., Burningham, B., et al. 2013, MNRAS, 434, 1005